Ab Initio Potential Energy Surface and Infrared Spectrum of the Ne−CO Complex

Robert Moszynski,*,† Tatiana Korona,† Paul E. S. Wormer,‡ and Ad van der Avoird‡

Department of Chemistry, University of Warsaw, Pasteura I, 02-093 Warsaw, Poland, and Institute of Theoretical Chemistry, NSR Center, University of Nijmegen, Toernooiveld 1, 6525 ED Nijmegen, The Netherlands

Received: March 6, 1997[⊗]

Symmetry-adapted perturbation theory has been applied to compute the intermolecular potential energy surface of the Ne−CO complex. The interaction energy is found to be dominated by the first-order exchange contribution and the dispersion energy. The *ab initio* potential has a single minimum of $\epsilon_m = -53.49$ cm^{-1} at $R_m = 6.34$ bohr and $\vartheta_m = 92.2°$. The computed potential energy surface has been analytically fitted and used in converged variational calculations to generate bound rovibrational states of the ^{20}Ne−CO complex and the infrared spectrum corresponding to the simultaneous excitation of vibration and internal rotation in the CO subunit within the complex. The computed frequencies of the infrared transitions corresponding to the $\Sigma \rightarrow \Sigma$, $\Sigma \rightarrow \Pi$, and $\Pi \rightarrow \Sigma$ subbands are in good agreement with the experimental data (Randall, R. W., *et al*. *Mol*. *Phys*. **1993**, *79*, 1113). The observed bending combination band is assigned to the transitions from the ground state to the first excited Σ state. Frequencies of the $\Pi \rightarrow \Delta$ and $\Delta \rightarrow \Pi$ transitions which were observed in the static cell spectrum are also reported.

I. Introduction

Theoretical and experimental studies of van der Waals complexes provide important information about weak intermolecular forces between atoms and molecules. Van der Waals molecules built of rare gas atoms and molecules are especially interesting, since they represent the simplest case of anisotropic interactions. The spectroscopic properties of these complexes range from those of a nearly free internal rotor (*e.g.*, Ar−H_2, ref 1) to those of an anharmonic oscillator/rigid rotor (*e.g.*, Ar−C_6H_6, refs 2 and 3). The complexes of CO with heavier rare gas atoms lie between the semirigid and nearly free internal rotor limits. They represent a very interesting intermediate case, where the assignments of the corresponding experimental spectra are rather difficult.

Theoretical and experimental investigations of the Ne−CO complex are scarce. To our knowledge no *ab initio* potential is available for this system. Until recently, experimental studies of Ne−CO were restricted to bulk and transport properties: second virial coefficients,[4,5] viscosity,[6] diffusion coefficients, and thermal diffusion factors.[7] These data were analyzed by using simple isotropic potentials. In 1993 Randall *et al*.[8] reported an experimental study of the infrared spectrum of Ne−CO corresponding to the simultaneous excitation of vibration and internal rotation of the CO subunit within the complex. Part of the recorded spectrum could be assigned by fitting the observed transition frequencies to a near-symmetric-rotor expression for the energy levels. The next step toward a full understanding of the dynamics of Ne−CO involves an analysis of the experimental data using a realistic potential energy surface, *e.g.*, from *ab initio* calculations.

In the present paper we report symmetry-adapted perturbation theory (SAPT) calculations of the potential energy surface for Ne−CO and dynamical calculations of the positions and intensities of lines in the infrared spectrum of the complex corresponding to the simultaneous excitation of vibration and internal rotation of the CO subunit within the complex. The plan of this paper is as follows. In section II the SAPT calculations are briefly described, and the analytical fits to the computed points are presented. In section III we describe the features of the computed potential energy surface. The formalism used in dynamical calculations is outlined in section IV. The calculated bound states and infrared spectrum are discussed in section V. Finally, in section VI we present conclusions.

II. Outline of SAPT Calculations

A. Method and Definitions. In the present paper we follow the approach introduced and tested in our previous papers[9−12] (see also ref 13 for a review). The SAPT interaction energy is represented as a double perturbation expansion of various polarization and exchange contributions,[14,15]

$$E_{int} = \sum_{n=1}^{\infty}\sum_{l=0}^{\infty}(E_{pol}^{(nl)} + E_{exch}^{(nl)}) \tag{1}$$

where $E_{pol}^{(nl)}$ and $E_{exch}^{(nl)}$ denote polarization and exchange contributions, respectively, of the nth-order in the intermolecular interaction and lth-order in the intramonomer electronic correlation. For the purpose of further discussion it is convenient to introduce a partitioning of E_{int} into components corresponding to the Hartree−Fock (E_{int}^{HF}) and correlated (E_{int}^{corr}) levels of the theory,

$$E_{int} = E_{int}^{HF} + E_{int}^{corr} \tag{2}$$

The Hartree−Fock interaction energy is decomposed as[16−19]

$$E_{int}^{HF} = E_{pol}^{(10)} + E_{exch}^{(10)} + E_{ind,resp}^{(20)} + E_{exch-ind,resp}^{(20)} + \delta E_{int}^{HF} \tag{3}$$

where $E_{pol}^{(10)}$ and $E_{exch}^{(10)}$ are the electrostatic and exchange contributions, respectively, with complete neglect of the intramolecular correlation effects,[20] $E_{ind,resp}^{(20)}$ and $E_{exch-ind,resp}^{(20)}$ are the Hartree−Fock induction and exchange-induction energies, respectively, accounting for the coupled-Hartree−Fock type response,[18,19] and δE_{int}^{HF} collects higher-order induction and exchange contributions. For the Ne−CO interaction at large

* To whom correspondence should be addressed.
† University of Warsaw.
‡ University of Nijmegen.
⊗ Abstract published in *Advance ACS Abstracts,* June 1, 1997.

S1089-5639(97)00855-4 CCC: $14.00

TABLE 1: Convergence of the Many-Body Perturbation Expansions of the Electrostatic, Exchange, Induction, and Dispersion Components of the Interaction Energy, for R = 7.0 bohr and $\vartheta = 90°$[a]

$E_{pol}^{(10)}$	−4.581	$E_{ind,resp}^{(20)}$	−4.912
$E_{pol,resp}^{(12)}$	−1.954	$\epsilon_{ind}^{(22)}$	−0.966
$E_{pol,resp}^{(13)}$	0.820	$E_{disp}^{(20)}$	−48.849
$E_{exch}^{(10)}$	17.208	$E_{disp}^{(21)}$	2.294
$\epsilon_{exch}^{(1)}$(CCSD)	3.723	$E_{disp}^{(22)}$	−10.229

[a] Energies are in cm^{-1}.

intermonomer distances R the latter term is dominated by the third-order induction energy and vanishes as R^{-10}.

At the correlated level, the SAPT interaction energy is represented by

$$E_{int}^{corr} = \epsilon_{pol}^{(1)} + \epsilon_{exch}^{(1)} + \epsilon_{ind}^{(2)} + \epsilon_{exch-ind}^{(2)} + E_{disp}^{(2)} + E_{exch-disp}^{(2)} \quad (4)$$

where $E_{disp}^{(2)}$ is the exact dispersion energy, and $\epsilon_{pol}^{(1)}$, $\epsilon_{exch}^{(1)}$, $\epsilon_{ind}^{(2)}$, $\epsilon_{exch-ind}^{(2)}$ are the electron correlation contributions to the exact electrostatic ($E_{pol}^{(1)}$), exchange ($E_{exch}^{(1)}$), induction ($E_{ind}^{(2)}$), and exchange-induction ($E_{exch-ind}^{(2)}$) energies, respectively, *i.e.*, $\epsilon_{pol}^{(1)} \equiv E_{pol}^{(1)} - E_{pol}^{(10)}$, $\epsilon_{exch}^{(1)} \equiv E_{exch}^{(1)} - E_{exch}^{(10)}$, and $\epsilon_{ind}^{(2)} \equiv E_{ind}^{(2)} - E_{ind,resp}^{(20)}$, and $\epsilon_{exch-ind}^{(20)} \equiv E_{exch-ind}^{(2)} - E_{exch-ind,resp}^{(20)}$. In the present study the contributions to E_{int}^{corr} were approximated as follows:

$$\epsilon_{pol}^{(1)} = E_{pol,resp}^{(12)} + E_{pol,resp}^{(13)} \quad (5)$$

$$\epsilon_{exch}^{(1)} = E_{exch}^{(11)} + E_{exch}^{(12)} + \Delta_{exch}^{(1)}(\text{CCSD}) \quad (6)$$

$$\epsilon_{ind}^{(2)} = \epsilon_{ind}^{(22)} \quad (7)$$

$$E_{disp}^{(2)} = E_{disp}^{(20)} + E_{disp}^{(21)} + E_{disp}^{(22)} \quad (8)$$

$$E_{exch-disp}^{(2)} = E_{exch-disp}^{(20)} \quad (9)$$

The electrostatic corrections $E_{pol,resp}^{(1n)}$ are defined as in ref 21. The first-order exchange components $E_{exch}^{(1n)}$ are defined as in refs 22 and 23. The quantity $\Delta_{exch}^{(1)}$(CCSD), obtained from coupled cluster singles and doubles calculations, gives first-order exchange contributions of higher than second-order in the monomer correlation. The dispersion components $E_{disp}^{(2n)}$ are derived in ref 24. The induction-correlation term $\epsilon_{ind}^{(22)}$ represents the true correlation contribution to the nonrelaxed $E_{ind}^{(22)}$ correction, as defined in ref 25. Finally, $E_{exch-disp}^{(20)}$ is the so-called "Hartree−Fock" exchange-dispersion energy.[26]

The uncorrelated induction energy $E_{ind,resp}^{(20)}$ is significantly quenched by its exchange counterpart and the same must be true in the case of $\epsilon_{ind}^{(22)}$. Thus, the inclusion of this term without the corresponding exchange contribution would not be appropriate. Since the contribution which accounts for such quenching has not been coded yet, we have estimated it by scaling the uncorrelated quantity with the factor $\epsilon_{ind}^{(22)}/E_{ind,resp}^{(20)}$,[27]

$$\epsilon_{exch-ind}^{(2)} \approx E_{exch-ind,resp}^{(20)} \frac{\epsilon_{ind}^{(22)}}{E_{ind,resp}^{(20)}} \quad (10)$$

As shown in Table 1, the convergence in terms of the intramolecular correlation is very good for the electrostatic, first-order exchange and induction energies, and the approximations given by eqs 5−7 should be accurate within a few percent. The convergence of the many-body perturbation expansion of the dispersion energy is only moderately fast. However, the results of refs 28 and 29 suggest that the contribution of terms of the order higher than the second ($n \geq 3$) should represent at worst a few percent of the total dispersion energy.

B. Computational Details. The intermolecular potential energy surface for the Ne−CO system, where CO is kept rigid, can be naturally described in the Jacobi coordinates (R,ϑ), where R is the distance from the center of mass of CO to the Ne atom, and ϑ is the angle between the vector pointing from the center of mass of CO to Ne and the vector pointing from the carbon to the oxygen atom. Calculations have been performed for five intermolecular distances R ranging from $R = 5$ bohr to $R = 10$ bohr and seven equidistant angles ϑ from $\vartheta = 0°$ to $\vartheta = 180°$. In addition, potential energy curves for $\vartheta = 15°$, 75°, 105°, and 165° have been computed. In total, we calculated 55 points on the surface. In all calculations the bond length of CO was fixed at its experimental equilibrium value, *i.e.*, r(CO) = 2.132 bohr. For the neon atom we used a [5s4p3d2f] basis set. The core-valence part of this basis consisted of the cc-pVDZ basis of Woon and Dunning[30,31] with the most diffuse s exponent (0.4869) left uncontracted. For the diffuse part we selected an even-tempered set optimized for the cc-pVTZ basis.[32] We augmented this basis with s orbitals with exponents 0.1133 and 0.033 94, p orbitals (0.0918 and 0.025 52), d orbitals (0.386 and 0.135 95), and f orbitals (1.084 and 0.461 89) (see Table III of ref 32). For the CO monomer we used the [8s5p3d1f/8s5p3d1f] basis set of Diercksen and Sadlej[33] optimized for dipole and quadrupole properties of this molecule. The spherical form of the polarization functions has been used (five d functions and seven f functions). In order to fully account for the charge-overlap effects all calculations have been done by using the full dimer basis set.

All calculations have been performed with the SAPT system of codes.[34] In addition, long-range induction and dispersion coefficients corresponding to the multipole-expanded induction[35] and dispersion energies[10] have been computed at the same level of theory and with the same basis sets by means of the Polcor package.[36,37] These coefficients have been subsequently used in the analytical fits of the induction and dispersion energies. We used the Boys−Bernardi counterpoise correction to eliminate the basis set superposition error from the supermolecular Hartree−Fock calculations.[38]

C. Analytical Potential Fits. The different contributions to the interaction energy, as computed by SAPT, exhibit different radial dependence, and each component of the interaction energy can be fitted separately. The fitting procedure adopted in the present work was the same as in our previous papers.[11,12] Below, we give only a short summary. For the details we refer the reader to ref 12.

We performed separate fits of the sum of short-range contributions E_{short},

$$E_{short} = E_{pol}^{(1)} + E_{exch}^{(1)} + E_{exch-ind}^{(2)} + E_{exch-disp}^{(2)} + \delta E_{int}^{HF} \quad (11)$$

of the induction energy $E_{ind}^{(2)}$, and of the dispersion energy $E_{disp}^{(2)}$. The short-range contribution was fitted to the expression

$$E_{short}(R,\vartheta) = \exp(-\alpha(\vartheta)[R - R_0^{sh}(\vartheta)]) - R\exp(-\alpha(\vartheta)[R - R_1^{sh}(\vartheta)]) \quad (12)$$

where the parameters $\alpha(\vartheta)$, $R_0^{sh}(\vartheta)$, and $R_1^{sh}(\vartheta)$ were represented by Legendre expansions,

$$\alpha(\vartheta) = \sum_{l=0}^{l_{max}} \alpha_l P_l(\cos\vartheta), \quad R_0^{sh}(\vartheta) = \sum_{l=0}^{l_{max}} R_{0l}^{sh} P_l(\cos\vartheta),$$

$$R_1^{sh}(\vartheta) = \sum_{l=0}^{l_{max}} R_{1l}^{sh} P_l(\cos\vartheta) \quad (13)$$

Note that we use atomic units for the energy, as well as for the distance.

The induction component $E_{ind}^{(2)}(R,\vartheta)$ was represented by the sum of the damped multipole expansion and an exponential function (the latter representing the short-range charge-overlap contribution to the induction energy[39−41]

$$E_{ind}^{(2)}(R,\vartheta) = \exp(-\beta^{ind}(\vartheta)[R - R_0^{ind}(\vartheta)]) - \sum_{n=6}^{12} f_n(R; \tilde{\beta}^{ind}(\vartheta))\, C_{n,ind}(\vartheta) R^{-n} \quad (14)$$

The induction constants for a given ϑ are defined by

$$C_{n,ind}(\vartheta) = \sum_{l=0}^{n-4} C_{n,ind}^{l} P_l(\cos\vartheta) \quad (15)$$

where $C_{n,ind}^{l}$ are standard long-range induction coefficients as defined in ref 35. The coefficients $C_{n,ind}^{l}$ were computed *ab initio* in the same basis set and at the level of theory corresponding to the fitted function $E_{ind}^{(2)}(R,\vartheta)$. We assumed the damping function $f_n(R;b)$ in the Tang−Toennies form.[42] Similarly as in the case of the E_{short} component, the fitted parameters $\beta^{ind}(\vartheta)$, $R_0^{ind}(\vartheta)$, and $\tilde{\beta}^{ind}(\vartheta)$ were represented by series in Legendre polynomials.

The analytical representation of the dispersion energy was the same as of the induction term, eq 14, with the induction constants $C_{n,ind}(\vartheta)$ replaced by the dispersion constants $C_{n,disp}(\vartheta)$. The long-range dispersion coefficients were again computed *ab initio* in the same basis set and at the level of theory corresponding to the fitted function $E_{disp}^{(2)}(R,\vartheta)$. The damping function was also assumed in the Tang−Toennies form.

In all fits the agreement between computed and fitted points was very good: typical deviations are of the order of 0.5% and—except for the region where the potential vanishes—the error did nowhere exceed 1%. We have not tabulated all the fit parameters; a Fortran program that generates the analytical Ne−CO potential can be requested by e-mail from avda@theochem.kun.nl.

III. Features of the Potential Energy Surface

The computed potential energy surface for Ne−CO reveals a single minimum of $\epsilon_m = -53.49$ cm^{-1} corresponding to the T-shape geometry of the complex ($R_m = 6.34$ bohr and $\vartheta_m = 92.2°$). The total interaction energy and its dominant components (E_{short}, $E_{ind}^{(2)}$, and $E_{disp}^{(2)}$) for $R = 7$ bohr and varying ϑ are shown in Figure 1. An inspection of Figure 1 shows that the short-range energy and the dispersion energy are two major contributions to the interaction potential determining its anisotropy. The induction energy is much less important for $\vartheta \leq 120°$ but shows a strong anisotropy for larger ϑ. Obviously, the dispersion and induction components favor the linear Ne−CO geometry. However, the short-range energy (dominated by the exchange energy, *cf.* Table 1) behaves, to a good approximation, in an opposite manner to $E_{disp}^{(2)} + E_{ind}^{(2)}$ and shows a stronger anisotropy. Consequently, the position of the minimum is determined by the anisotropy of the exchange-repulsion term.

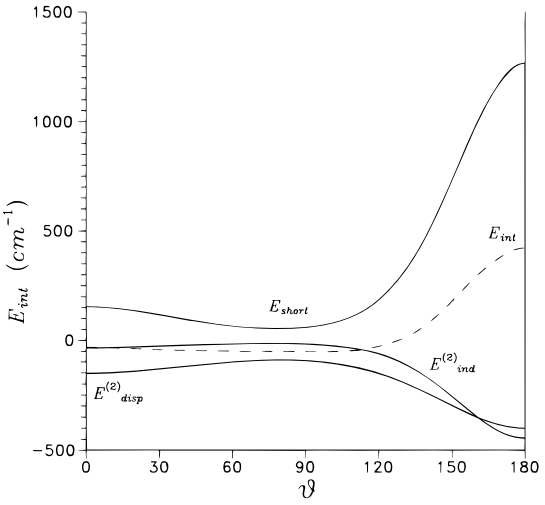

Figure 1. Angular dependence of the Ne−CO interaction energy components in the region of the van der Waals minimum ($R = 7.0$ bohr).

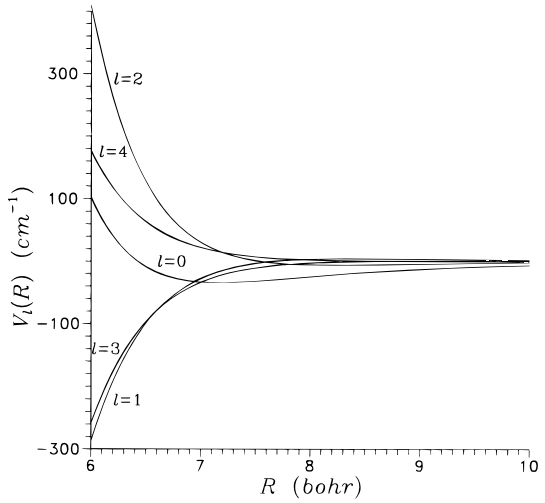

Figure 2. Expansion coefficients $V_l(R)$, *cf.* eq 16, of the *ab initio* Ne−CO interaction potential.

In Figure 1 we also report the angular scan of the potential energy surface in the region of the van der Waals minimum. An inspection of this figure shows that the potential is rather flat as function of the angle for $\vartheta \leq 120°$ and shows a high barrier to internal rotation of the CO subunit around $\vartheta = 180°$. This strongly suggests that the CO monomer in the complex will behave like a hindered rotor.

To investigate the importance of the anisotropic contributions to the potential in various regions of the configuration space it is useful to expand it as a series in Legendre polynomials

$$V(R,\vartheta) = \sum_{l=0}^{\infty} V_l(R) P_l(\cos\vartheta) \quad (16)$$

where V is the sum of contributions in eqs 12 and 14 and the dispersion equivalent of eq 14. The expansion coefficients $V_l(R)$ can be easily evaluated numerically by the use of the Gauss−Legendre quadrature. The advantage of the expansion (16) is that it shows explicitly the anisotropy of the potential, the term with $l = 0$ being the isotropic potential. In order to establish the importance of various anisotropic terms at various R, we report in Figure 2 the radial dependence of the $V_l(R)$ coefficients for $l \leq 4$. Around the van der Waals minimum ($R = 6.34$ bohr) all terms up to $l = 4$ contribute significantly to the potential,

and a closer analysis shows that higher anisotropic terms are also important, and in order to obtain converged results for ϑ varying from 0° to 180°, one has to sum up all terms up to and including $l = 14$. At the minimum this expansion approximates the total energy within 1%. The fact that we need to go to this high order in l also suggests that the rotations of the CO subunit within the dimer will be hindered.

As discussed in the Introduction, the transport data of the Ne−CO mixtures could be analyzed in terms of simple isotropic potentials,[6,7] so it is interesting to compare these potentials with the *ab initio* isotropic potential. The empirical potential fitted[7] to the diffusion data and second virial coefficients has a minimum of $\epsilon_{0m} = -43.09$ cm^{-1} at $R_{0m} = 6.36$ bohr, and crosses zero at $\sigma = 5.77$ bohr. These values do not compare favorably with the parameters of the *ab initio* isotropic potential: $\epsilon_{0m} = -34.42$ cm^{-1}, $R_{0m} = 7.16$ bohr, and $\sigma = 6.43$ bohr. Since our full *ab initio* potential reproduces very well[43] the measured second virial coefficients,[4,5] it seems that the isotropic potential derived in ref 7 is an effective potential and represents a poor approximation to the true isotropic potential. By contrast, our values of ϵ_{0m} and σ agree rather well with the scaling parameters $\epsilon_{ij} = -36.09$ cm^{-1} and $\sigma_{ij} = 6.16$ bohr for Ne−CO, applied in the analysis of the viscosity data using the extended law of corresponding states.[6]

IV. Outline of the Dynamical Calculations

Depending on the strength of the anisotropy in the interaction potential, nuclear motions in weakly bound van der Waals complexes are usually described by using a set of coordinates related to a space-fixed or body-fixed frame.[44] The semiempirical analysis of the experimental spectrum reported in ref 8 suggests that a body-fixed description is appropriate. This means that the energy levels and infrared transitions can be approximately classified by using the case *b* coupling of Bratoz and Martin;[45] *i.e*., the diatom in the complex should behave as a hindered rotor. Choosing the *embedded* reference frame such that the vector $\boldsymbol{R}$ connecting the diatom center of mass with the atom defines the new z axis, the Hamiltonian describing the nuclear motion can be written as[46,47]

$$H = -\frac{\hbar^2}{2\mu R}\frac{\partial^2}{\partial R^2}R + \frac{\boldsymbol{J}^2 + \boldsymbol{j}^2 - 2\boldsymbol{j}\cdot\bar{\boldsymbol{J}}}{2\mu R^2} + b_v\boldsymbol{j}^2 + V \quad (17)$$

Here, the operator $\boldsymbol{j}$ acts on the angular coordinates of the vector $\boldsymbol{r}$ in the body-fixed frame. Note, that the present coordinate system corresponds to the so-called "two-thirds body-fixed" system of refs 44 and 47. Therefore, the angular momentum operator $\boldsymbol{j}$ and the pseudo angular momentum operator $\bar{\boldsymbol{J}}$ *do not* commute and $\bar{\boldsymbol{J}} \neq \boldsymbol{J}$.

The only rigorously conserved quantum numbers are the total angular momentum J and the spectroscopic parity σ. [The spectroscopic parity σ is related to the conventional parity p by the relation $\sigma = p(-1)^J$.] The diatom rotational quantum number j, and the projection K of $\boldsymbol{J}$ (and $\boldsymbol{j}$) onto the intermolecular axis, are only approximately conserved. This conservation is broken by off-diagonal Coriolis interaction. Since K is the projection of an angular momentum, states with $K = 0, \pm1$, *etc*., are denoted as Σ, Π, *etc*. In addition, levels with $\sigma = +1$ and $\sigma = -1$ will be designated by superscripts e and f, respectively. For $K = 0$ only e parity states exist. The case *b* coupling of Bratoz and Martin[45] gives a very simple classification of the rovibrational energy levels of the complex: each monomer rotational level j is split into $j + 1$ levels corresponding to any $J \geq |K|$ with $K = 0, \pm1, \pm2, ..., \pm j$. The inclusion of the Coriolis interaction introduces further splitting of the states with $|K| \neq 0$ (the so-called l-doubling) into states with e and f parity labels.

The wave function describing the nuclear motion can be expanded in a basis of products of radial functions $\chi_n(R)$ and angular functions of the form

$$[Y_K^j(\vartheta,\varphi)D_{M,K}^{(J)*}(\alpha,\beta,0) + \sigma Y_{-K}^j(\vartheta,\varphi)D_{M,-K}^{(J)*}(\alpha,\beta,0)] \quad (18)$$

where (β,α) are polar angles of the $\boldsymbol{R}$ vector in the space-fixed coordinates, ϑ and φ are the spherical angles of the $\boldsymbol{r}$ vector in the body-fixed coordinates, and $D_{M,K}^{(J)}(\alpha,\beta,\gamma)$ is an element of the Wigner rotation matrix.[48] The angular basis functions have a well-defined parity σ, so the full Hamiltonian, eq 17, is blocked in both σ and J. Within each block functions with different K are mixed through the off-diagonal Coriolis interaction.

The radial basis consisted of Morse-type oscillator functions[46] characterized by three parameters: R_e, D_e, and ω_e, which served as further variational parameters. We optimized these by minimizing the energy of the $J = 0$ state. This gave $R_e = 7.2$ bohr, and $D_e = 34.39$ cm^{-1}, and $\omega_e = 16.46$ cm^{-1}. The final basis was restricted to the space with $j \leq 14$ and $n \leq 20$. The rotational constants of the CO molecule were fixed at 1.922 516 5 and 1.905 013 5 cm^{-1} for ground and excited vibrational states, respectively. In the calculations we used the following masses: ^{49} ^{20}Ne − 19.992 44 amu, ^{12}C − 12.0 amu, and ^{16}O − 15.994 91 amu.

The allowed dipole transitions between the states of the complex can be deduced from an analysis of the expression for the transition intensity, and it follows easily that the observed dipole transitions must obey the following rigorous selection rules: $|\Delta J| = 1$, $\Delta\sigma = 0$ or $\Delta J = 0$, $|\Delta\sigma| = 2$. Since the K quantum number is nearly conserved, an additional approximate selection rule should hold: $|\Delta K| = 0, 1$.

The wave functions for the initial and final states obtained by solving the Schrödinger equation with the Hamiltonian of eq 17 can be used to compute the infrared absorption intensities for the complex. The infrared absorption coefficient $I(i''J'' \rightarrow i'J')$ for the transition $i''J'' \rightarrow i'J'$ is proportional to,

$$\frac{\exp\left(-E_{i''0}^{J''}/k_BT\right)}{Z(T)}\left(E_{i'1}^{J'} - E_{i''0}^{J''}\right)S(0i''J'' \rightarrow 1i'J') \quad (19)$$

where E_{iv}^J denotes the energy of the ith state of Ne−CO(v) labeled by J, $Z(T)$ is the partition function, the line strength is given by

$$S(0i''J'' \rightarrow 1i'J') = \sum_{M'',M',m}\left|\left\langle\Psi_{i'}^{J'M'}\middle|\mu_m^{01}\middle|\Psi_{i''}^{J''M''}\right\rangle\right|^2 \quad (20)$$

and μ_m^{01} is the spherical component of the vibrational transition dipole of the CO monomer.

V. Bound States and Infrared Spectrum of Ne−CO

In Table 2 we report the energy levels of the ^{20}Ne−CO complex for $J \leq 9$. The ground state of ^{20}Ne−CO is bound by 34.15 cm^{-1}. Also presented in this table is the labeling of the van der Waals states with the K quantum number. As we discussed above, the K quantum number is nearly conserved, and the van der Waals states can be described by the Σ, Π, *etc*. labels. As discussed in section III, the anisotropy of the Ne−CO potential in the region of the van der Waals minimum is relatively strong, so it is interesting to see if the energy levels of Ne−CO can be approximately labeled with the j quantum number. An analysis of the dominant contributions of the angular functions labeled by j to the wave function for a given

TABLE 2: Energy Levels (in cm^{-1}) of the ^{20}Ne−CO ($v = 0$) Complex, Calculated from the *ab Initio* Potential

J	Σ	Π^e	Π^f	Δ^e	Δ^f	Φ^e	Φ^f
0	−34.152						
	−25.899						
	−18.824						
1	−33.934	−30.544	−30.529				
	−25.683	−18.141	−18.281				
	−18.786	−13.050	−12.995				
2	−33.498	−30.124	−30.079	−23.111	−23.111		
	−25.252	−17.558	−17.840	−7.644	−7.643		
	−18.576	−12.782	−12.625				
3	−32.846	−29.495	−29.404	−22.479	−22.479	−11.795	−11.789
	−24.606	−16.772	−17.179	−7.030	−7.027		
	−18.173	−12.371	−12.081				
4	−31.977	−28.656	−28.506	−21.638	−21.637	−10.980	−10.958
	−23.747	−15.791	−16.300	−6.224	−6.214		
	−17.573	−11.807	−11.362				
5	−30.893	−27.610	−27.385	−20.589	−20.588	−9.963	−9.918
	−22.678	−14.617	−15.205	−5.235	−5.211		
	−16.776	−11.081	−10.468				
6	−29.596	−26.357	−26.044	−19.336	−19.331	−8.748	−8.671
	−21.399	−13.254	−13.895	−4.077	−4.025		
	−15.781	−10.189	−9.396				
7	−28.088	−24.898	−24.484	−17.880	−17.870	−7.339	−7.223
	−19.915	−11.707	−12.373	−2.673	−2.664		
	−14.590	−9.127	−8.144				
8	−26.372	−23.236	−22.706	−16.228	−16.205	−5.743	−5.576
	−18.229	−9.981	−10.644	−1.304	−1.136		
	−13.201	−7.891	−6.712				
9	−24.449	−21.372	−20.715	−14.387	−14.341	−3.971	−3.738
	−16.346	−8.086	−8.711	0.294	0.552		
	−11.611	−6.479	−5.100				

J suggests that j is strongly mixed by the anisotropic interaction. This confirms again that the CO subunit in the complex behaves as a hindered rotor.

Since the rovibrational states of Ne−CO reveal a hindered rotor behavior, it may be interesting to see the contour plots of the corresponding wave functions. In Figure 3a we depict the contour plot of the anisotropic potential, while in Figure 3b we report the contour plot of the ground-state wave function. The ground-state wave function shows a single maximum, fairly close to the position of the minimum in the potential but slightly shifted to larger R, cf., Figure 3a. The state is rather localized in the van der Waals stretch coordinate R. The expectation value $\langle R \rangle$ is 6.87 bohr, which is not far from the minimum of the interaction potential ($R_m = 6.34$ bohr). In the angular coordinate ϑ the state is more delocalized, especially toward the smaller values of ϑ. This may be seen from the spread in angles: the minimum value ϑ_m is 92.2°, the value $\arccos\langle P_1(\cos\vartheta)\rangle$ obtained from $\langle P_1 \rangle$ is 68.32°, and the value $\arccos[(2\langle P_2(\cos\vartheta)\rangle + 1)/3]^{1/2}$ obtained from $\langle P_2 \rangle$ is 57.09°.

The infrared transition frequencies for the ^{20}Ne−CO complex are reported in Tables 3−11 (see also Figure 4 for graphical illustrations of the spectra at $T = 2$ *K* and $T = 50$ *K*). Since we assumed that the CO vibration is decoupled from the intermolecular modes, the transition frequencies were computed from the formula

$$\Delta E(J' \rightarrow J'') = E_{i'_1}^{J'} - E_{i''_0}^{J''} + Q_1(0) \qquad (21)$$

where $Q_1(0) = 2143.2712$ cm^{-1} [50] is the frequency of the CO stretching fundamental.

An inspection of Table 3 shows that the agreement of theoretical transition frequencies for the $\Sigma \rightarrow \Sigma$ subband with the results of high-resolution measurements is very good. Since the $\Sigma \rightarrow \Sigma$ transitions probe mainly the isotropic potential and its dependence on r(CO), the level of agreement presented in Table 3 suggests that the isotropic part of the *ab initio* potential is accurate. Small discrepancies of the order of 0.07 cm^{-1} may

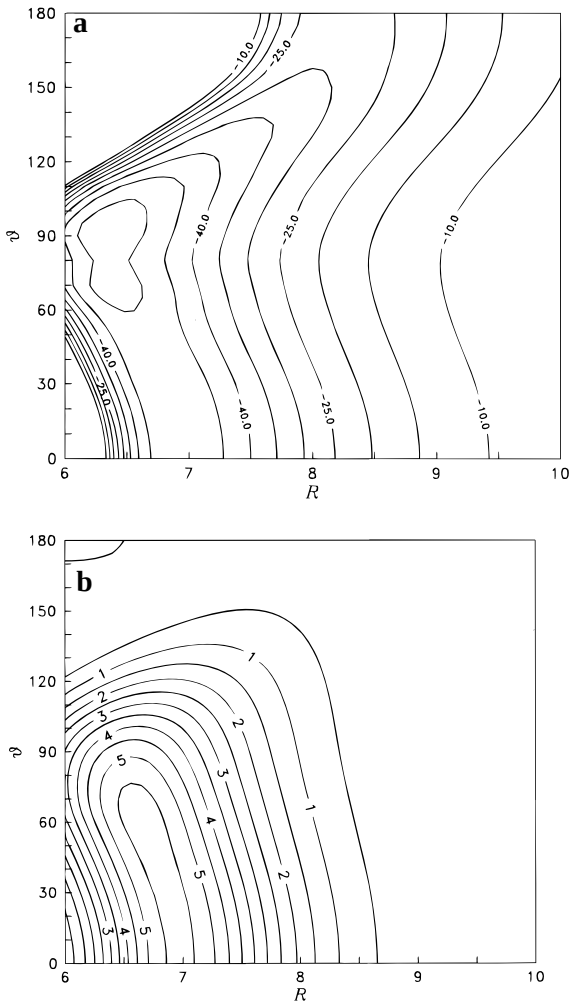

Figure 3. (a) Cut through the *ab initio* Ne−CO potential (in cm^{-1}). (b) Cut through the $J = 0$, $j = 0$ rovibrational wave function of Ne−CO($v = 0$), amplitude in 10^{-3} (bohr)$^{-3/2}$.

TABLE 3: Frequencies (in cm^{-1}) of the Infrared Transitions in the $\Sigma \rightarrow \Sigma$ Subband of the ^{20}Ne−CO Spectrum[a]

	P(*J*)			*R*(*J*)		
J	theory	experiment	Δ	theory	experiment	Δ
0				2143.4770	2143.4171	0.060 (0.011)
1	2143.0409	2142.9827	0.058 (0.006)	2143.6947	2143.6337	0.061 (0.014)
2	2142.8232	2142.7653	0.058 (0.004)	2143.9118	2143.8494	0.062 (0.017)
3	2142.6061	2142.5485	0.058 (0.003)	2144.1278	2144.0637	0.064 (0.021)
4	2142.3900	2142.3319	0.058 (0.002)	2144.3426	2144.2768	0.066 (0.024)
5	2142.1751	2142.1163	0.059 (0.002)	2144.5556	2144.4870	0.069 (0.029)
6	2141.9620	2141.9019	0.060 (0.002)	2144.7665	2144.6974	0.069 (0.032)
7	2141.7508	2141.6889	0.062 (0.003)	2144.9751	2144.9020	0.073 (0.038)
8	2141.5420	2141.4791	0.063 (0.004)	2145.1807	2145.1050	0.076 (0.043)
9	2141.3360	2141.2711	0.065 (0.005)			

[a] Δ is the absolute error of the transition frequencies computed from the *ab initio* potential. The numbers in parentheses are absolute errors of the transition frequencies computed from the scaled potential.

TABLE 4: Frequencies (in cm^{-1}) of the Infrared Transitions in the $\Sigma \rightarrow \Pi^e$ Subband of the ^{20}Ne−CO Spectrum[a]

	P(*J*)			*R*(*J*)		
J	theory	experiment	Δ	theory	experiment	Δ
0				2146.8332	2146.5947	0.238 (−0.024)
1				2147.0350	2146.7933	0.242 (−0.019)
2	2146.1794	2145.9427	0.237 (−0.031)	2147.2286	2146.9821	0.246 (−0.012)
3	2145.9464	2145.7078	0.239 (−0.030)	2147.4138	2147.1604	0.253 (−0.002)
4	2145.7068	2145.4644	0.242 (−0.027)	2147.5909	2147.3288	0.262 (0.009)
5	2145.4611	2145.2133	0.248 (−0.022)	2147.7600	2147.4865	0.274 (0.023)
6	2145.2103	2144.9546	0.256 (−0.014)	2147.9215	2147.6336	0.288 (0.040)
7	2144.9552	2144.6893	0.266 (−0.004)	2148.0756	2147.7691	0.306 (0.060)
8	2144.6969	2144.4165	0.280 (0.010)	2148.2227	2147.8927	0.330 (0.086)
9	2144.4365	2144.1380	0.298 (0.028)			

[a] Δ is the absolute error of the transition frequencies computed from the *ab initio* potential. The numbers in parentheses are absolute errors of the transition frequencies computed from the scaled potential.

TABLE 5: Frequencies (in cm^{-1}) of the Infrared Transitions in the $\Sigma \rightarrow \Pi^f$ Subband of the ^{20}Ne−CO Spectrum[a]

	Q(*J*)				*Q*(*J*)		
J	theory	experiment	Δ	*J*	theory	experiment	Δ
1	2146.6304	2146.3921	0.238 (−0.027)	6	2146.7775	2146.5038	0.274 (0.002)
2	2146.6449	2146.4033	0.242 (−0.024)	7	2146.8302	2146.5430	0.287 (0.014)
3	2146.6667	2146.4192	0.247 (−0.019)	8	2146.8910	2146.5877	0.303 (0.028)
4	2146.6960	2146.4421	0.254 (−0.014)	9	2146.9603	2146.6391	0.321 (0.043)
5	2146.7329	2146.4701	0.263 (−0.007)				

[a] Δ is the absolute error of the transition frequencies computed from the *ab initio* potential. The numbers in parentheses are absolute errors of the transition frequencies computed from the scaled potential.

TABLE 6: Frequencies (in cm^{-1}) of the Infrared Transitions in the $\Pi^e \rightarrow \Sigma$ Subband of the ^{20}Ne−CO Spectrum[a]

	P(*J*)			*R*(*J*)		
J	theory	experiment	Δ	theory	experiment	Δ
1	2139.6509	2139.7761	−0.125 (0.036)	2140.3047	2140.4222	−0.118 (0.048)
2	2139.4489	2139.5753	−0.126 (0.033)	2140.5375	2140.6599	−0.122 (0.045)
3	2139.2552	2139.3852	−0.130 (0.027)	2140.7769	2140.8995	−0.123 (0.046)
4	2139.0697	2139.2044	−0.135 (0.021)	2141.0222	2141.1484	−0.126 (0.044)
5	2138.8923	2139.0335	−0.141 (0.012)	2141.2727	2141.4047	−0.132 (0.039)
6	2138.7228	2138.8726	−0.150 (0.002)	2141.5274	2141.6660	−0.139 (0.034)
7	2138.5611	2138.7213	−0.160 (−0.009)	2141.7853	2141.9328	−0.147 (0.028)
8	2138.4066	2138.5830	−0.176 (−0.026)	2142.0453	2142.2072	−0.162 (0.016)
9	2138.2590	2138.4529	−0.194 (−0.043)			

[a] Δ is the absolute error of the transition frequencies computed from the *ab initio* potential. The numbers in parentheses are absolute errors of the transition frequencies computed from the scaled potential.

be due to the implicit use of the Ne−CO($v = 0$) potential for the CO($v = 1$) state in the bound state calculations.

Comparison of the theoretical and experimental frequencies of transitions between the Σ and Π states are presented in Tables 4−7. Here too, the agreement between theory and experiment is rather good. Most of the line positions agree within 0.1−0.3 cm^{-1} or better. Since the $\Sigma \rightarrow \Pi$ and $\Pi \rightarrow \Sigma$ transitions probe mainly the even anisotropic terms in the Legendre expansion of the interaction potential in eq 16 the results reported in Tables 4−7 show that the anisotropy of the *ab initio* potential is not entirely correct. The basis sets used in our SAPT calculation neglected the functions of g and higher symmetry. This neglect may affect both the dispersion energy and the first-order exchange-repulsion. It is not surprising, then, that the agreement with experiment is somewhat less satisfactory.

Since the results for the $\Sigma \rightarrow \Sigma$ transitions suggest that the potentials for Ne−CO($v = 0$) and Ne−CO($v = 1$) are slightly different, we repeated bound-state calculations using two potentials corresponding to the $v = 0$ and $v = 1$ states of CO. The potential for Ne−CO($v = 1$) was obtained by scaling the

TABLE 7: Frequencies (in cm^{-1}) of the Infrared Transitions in the $\Pi^f \rightarrow \Sigma$ Subband of the ^{20}Ne−CO Spectrum[a]

	$Q(J)$				$Q(J)$		
J	theory	experiment	Δ	J	theory	experiment	Δ
1	2139.8538	2139.9781	−0.124 (0.039)	6	2139.7067	2139.8560	−0.149 (0.024)
2	2139.8393	2139.9663	−0.127 (0.037)	7	2139.6541	2139.8127	−0.159 (0.019)
3	2139.8175	2139.9481	−0.131 (0.035)	8	2139.5932	2139.7626	−0.169 (0.012)
4	2139.7882	2139.9233	−0.135 (0.033)	9	2139.5239	2139.7083	−0.184 (0.002)
5	2139.7514	2139.8932	−0.142 (0.029)				

[a] Δ is the absolute error of the transition frequencies computed from the *ab initio* potential. The numbers in parentheses are absolute errors of the transition frequencies computed from the scaled potential.

TABLE 8: Frequencies (in cm^{-1}) of the Infrared Transitions in the $\Sigma \rightarrow \Sigma^{excited}$ Subband of the ^{20}Ne−CO Spectrum[a]

	$P(J)$			$R(J)$		
J	theory	experiment	Δ	theory	experiment	Δ
0				2151.6719	2151.9018	−0.230 (−0.017)
1	2151.2380	2151.4735	−0.236 (−0.023)	2151.8852	2152.1060	−0.221 (−0.013)
2	2151.0181	2151.2498	−0.232 (−0.023)	2152.0952		
3	2150.7965	2151.0206	−0.224 (−0.024)	2152.3010		
4	2150.5733	2150.7855	−0.212 (−0.023)	2152.5017		
5	2150.3483			2152.6962		
6	2150.1211			2152.8828		
7	2149.8914			2153.0602		
8	2149.6583			2153.2262		
9	2149.4211					

[a] Δ is the absolute error of the transition frequencies computed from the *ab initio* potential. The numbers in parentheses are absolute errors of the transition frequencies computed from the scaled potential.

TABLE 9: Frequencies (in cm^{-1}) of the Infrared Transitions in the $\Sigma^{excited} \rightarrow \Sigma$ Subband of the ^{20}Ne−CO Spectrum, Computed from the Scaled Potential

J	$P(J)$	$R(J)$	J	$P(J)$	$R(J)$
0		2134.9123	5	2133.6904	2136.0886
1	2134.4785	2135.1372	6	2133.5156	2136.3411
2	2134.2703	2135.3671	7	2133.3520	2136.6003
3	2134.0689	2135.6021	8	2133.2014	2136.8669
4	2133.8753	2135.8425	9	2133.0652	

TABLE 10: Frequencies (in cm^{-1}) of the Infrared Transitions in the $\Pi \rightarrow \Delta$ Subband of the ^{20}Ne−CO Spectrum, Computed from the Scaled Potential

	$\Pi^e \rightarrow \Delta^e$		$\Pi^e \rightarrow \Delta^f$	$\Pi^f \rightarrow \Delta^f$		$\Pi^f \rightarrow \Delta^e$
J	$P(J)$	$R(J)$	$Q(J)$	$P(J)$	$R(J)$	$Q(J)$
1		2150.4486			2150.4340	
2		2150.6648	2150.0249		2150.6206	2149.9817
3	2149.3905	2150.8824	2150.0294	2149.3036	2150.7394	2149.9435
4	2149.1851	2151.1011	2150.0350	2149.0401	2150.9521	2149.8931
5	2148.9828	2151.3207	2150.0418	2148.7648	2151.0962	2149.8309
6	2148.7839	2151.5401	2150.0492	2148.4781	2151.2254	2149.7570
7	2148.5887	2151.7573	2150.0571	2148.1802	2151.3393	2149.6711
8	2148.3968	2151.9686	2150.0650	2147.8714	2151.4371	2149.5716
9	2148.2067		2150.0722	2147.5521		2149.4557

TABLE 11: Frequencies (in cm^{-1}) of the Infrared Transitions in the $\Delta \rightarrow \Pi$ Subband of the ^{20}Ne−CO Spectrum, Computed from the Scaled Potential

	$\Delta^e \rightarrow \Pi^e$		$\Delta^e \rightarrow \Pi^f$	$\Delta^f \rightarrow \Pi^f$		$\Delta^f \rightarrow \Pi^e$
J	$P(J)$	$R(J)$	$Q(J)$	$P(J)$	$R(J)$	$Q(J)$
2	2135.8312	2136.8896	2136.2984	2135.8458	2136.9769	2136.2549
3	2135.6154	2137.0954	2136.3374	2135.6597	2137.2412	2136.2509
4	2135.3985	2137.2985	2136.3888	2135.4876	2137.5173	2136.2456
5	2135.1807	2137.4985	2136.4524	2135.3299	2137.8052	2136.2396
6	2134.9627	2137.6954	2136.5283	2135.1869	2138.1046	2136.2230
7	2134.7456	2137.8898	2136.6172	2135.0591	2138.4150	2136.2262
8	2134.5317	2138.0835	2136.7205	2134.9470	2138.7363	2136.2196
9	2134.3250		2136.8417	2134.8510		2136.2140

parameter α_0 by 0.9999 (*cf.* eq 13). In addition, to improve the agreement with the experimental transition frequencies for the $\Sigma \rightarrow \Pi$ and $\Pi \rightarrow \Sigma$ transitions we scaled in both potentials α_2 by a factor 1.015. The scaling parameters were chosen to reproduce the $J = 0 \rightarrow J = 1$ transitions in the $\Sigma \rightarrow \Sigma$ and $\Sigma \rightarrow \Pi$ bands.

The results computed from the two scaled surfaces for the $\Sigma \rightarrow \Sigma$ transitions are presented in Table 3 in parentheses. An inspection of Table 3 shows that this scaling greatly improves the agreement between theory and experiment and supports our conclusion that the potential for Ne−CO($v = 1$) is slightly different from the one for Ne−CO($v = 0$). Similar results for

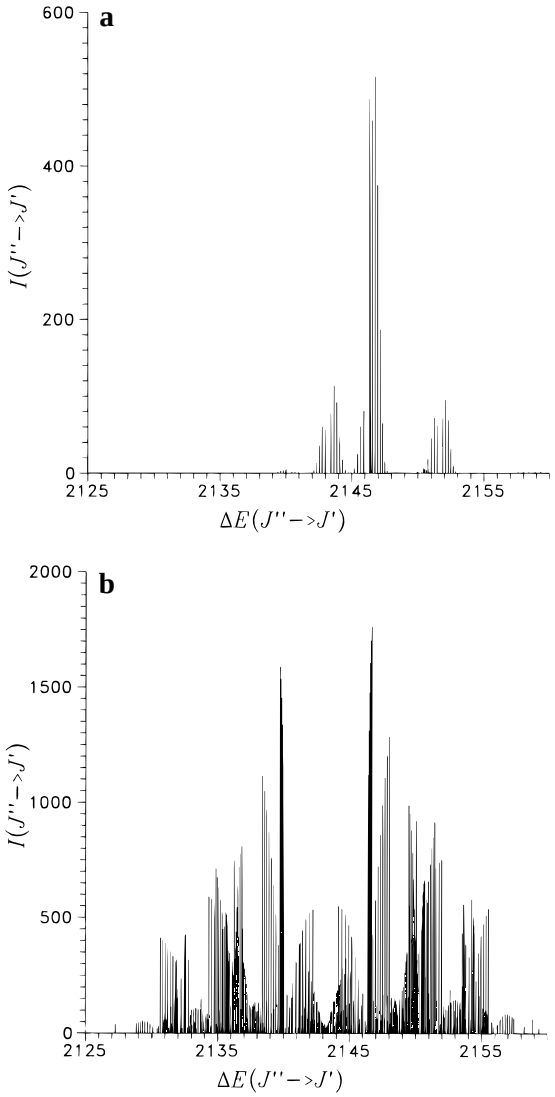

Figure 4. Theoretical infrared spectra of the ^{20}Ne−CO complex accompanying the fundamental band of CO. The temperature is (a) 2 K and (b) 50 K.

the $\Sigma \rightarrow \Pi$ and $\Pi \rightarrow \Sigma$ subbands are shown in Tables 4−7. Here too, the agreement with the experiment is greatly improved (by an order of magnitude or better). The absolute error of the theoretical transition frequencies is of the order of 0.05 cm^{-1}. It is worth noting that we did not attempt to fit systematically the potential to the experimental spectrum but simply checked if by a simple scaling we could obtain better agreement with experiment.

Randall *et al.*[8] also reported observations of an additional band in the region of 2151 cm^{-1} which was tentatively assigned as a bending combination band. The results of the theoretical calculations corresponding to this region presented in Table 8 show that this band corresponds to transitions from the ground Σ state of Ne−CO($v = 0$) to the first excited Σ state of Ne−CO($v = 1$). Also for this band the agreement between theory and experiment is satisfactory (within 0.2 cm^{-1}), and the scaling reduces the absolute error by a factor of 10.

Having the assignment for the observed bending combination band it is interesting to check whether the final states in this band can indeed be considered as bending states. In Figure 5a we present the plot of the wave function for the excited Σ state with $J = 0$. An inspection of this figure shows that the wave function for this state has a nodal surface almost parallel to the R axis. Hence, the first excited Σ state can be considered as a

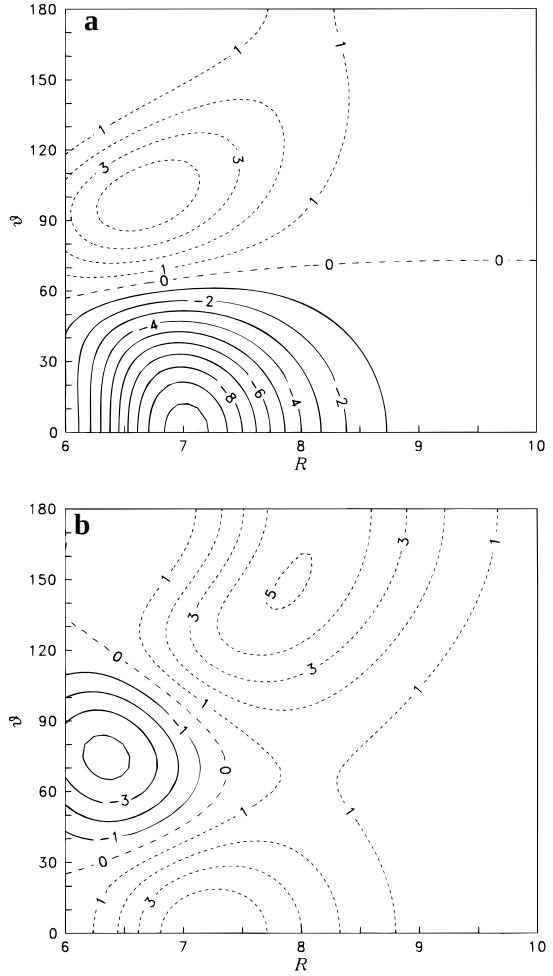

Figure 5. (a) Cut through the first excited rovibrational wave function of Ne−CO($v = 0$) for $J = 0$, amplitude in 10^{-3} (bohr)$^{-3/2}$. (b) Cut through the second excited rovibrational wave function of Ne−CO($v = 0$) for $J = 0$, amplitude in 10^{-3} (bohr)$^{-3/2}$.

bending vibrational state of the complex. It is interesting to note that the second excited Σ state cannot be associated with a simple bending/stretch mode. Figure 5b shows that the bending and stretch excitations are heavily mixed for this state.

Our computed spectrum at 50 K shows that additional transitions not reported in ref 8 should be observed in the static cell spectrum. These additional transitions will correspond (among others) to the excited $\Sigma \rightarrow$ ground Σ transitions and to $\Pi \rightarrow \Delta$ and $\Delta \rightarrow \Pi$ subbands. The corresponding transition frequencies computed from the scaled potential are reported in Tables 9−11. These data will be useful in assigning portions of the experimental spectrum in the region of 2133−2139 and 2149−2154 cm^{-1}.

VI. Summary and Conclusions

The interaction potential energy surface of the Ne−CO complex has been calculated for a broad range of configurations by the use of symmetry-adapted perturbation theory. From our calculations we extracted functions describing the separate components of the interaction energy. Using the computed potential energy surface we have generated bound rovibrational states and the infrared spectrum of the Ne−CO complex corresponding to the simultaneous excitation of the vibration and hindered rotation of the CO molecule within the dimer. Variational characterization of the rovibrational states revealed a ground state of ^{20}Ne−CO with a dissociation energy of 34.15 cm^{-1} and several rotationally excited states of the complex. The

computed frequencies of the infrared transitions corresponding to the $\Sigma \rightarrow \Sigma$, $\Sigma \rightarrow \Pi$, and $\Pi \rightarrow \Sigma$ subbands are in good agreement with the experimental data.[8] Still a minor improvement in the agreement between theory and experiment could be achieved by adjusting the anisotropy of the exchange-repulsion energy and by making the Ne−CO ($v = 1$) potential slightly different from the Ne−CO ($v = 0$) potential. Our calculations assigned the observed bending combination band to the transitions from the ground Σ state to the first excited Σ state. In addition, frequencies of the $\Pi \rightarrow \Delta$ and $\Delta \rightarrow \Pi$ transitions observed in the static cell spectrum were predicted.

Acknowledgment. We thank Robert McKellar for valuable discussions. This work was supported by the Netherlands Foundation of Chemical Research (SON), the Netherlands Organization for Scientific Research (NWO), and Polish Scientific Research Council (KBN) funds through the Department of Chemistry, University of Warsaw, within the grant BST-532/23/96.

References and Notes

(1) Moszynski, R.; Jeziorski, B.; Wormer, P. E. S.; van der Avoird, A. *Chem. Phys. Lett.* **1994**, *221*, 161.
(2) van der Avoird, A. *J. Chem. Phys.* **1993**, *98*, 5327.
(3) Riedle, E.; van der Avoird, A. *J. Chem. Phys.* **1996**, *104*, 882.
(4) Brewer, J. AFOSR Report No. MRL-2915-C, **1967**.
(5) Vatter, K.; Schmidt, H. J.; Elias, E.; Schramm, B. *Ber. Bunsenges. Phys. Chem.* **1996**, *100*, 73.
(6) Kestin, J.; Ro, S. T.; Wakeham, W. A. *Ber. Bunsenges. Phys. Chem.* **1982**, *86*, 753.
(7) Trengove, R. D.; Robjohns, H. L.; Dunlop, P. J. *Ber. Bunsenges. Phys. Chem.* **1984**, *88*, 450.
(8) Randall, R. W.; Cliffe, A. J.; Howard, B. J.; McKellar, A. R. W. *Mol. Phys.* **1993**, *79*, 1113.
(9) Williams, H. L.; Szalewicz, K.; Jeziorski, B.; Moszynski, R.; Rybak, S. *J. Chem. Phys.* **1993**, *98*, 1279.
(10) Moszynski, R.; Wormer, P. E. S.; Jeziorski, B.; van der Avoird, A. *J. Chem. Phys.* **1994**, *101*, 2811.
(11) Moszynski, R.; Wormer, P. E. S.; van der Avoird, A. *J. Chem. Phys.* **1995**, *102*, 8385.
(12) Moszynski, R.; Korona, T.; Wormer, P. E. S.; van der Avoird, A. *J. Chem. Phys.* **1995**, *102*, 321.
(13) Jeziorski, B.; Moszynski, R.; Szalewicz, K. *Chem. Rev.* **1994**, *94*, 1887.
(14) Jeziorski, B.; Kolos, W. *Int. J. Quantum Chem. (Suppl. 1)* **1977**, *12*, 91.
(15) Szalewicz, K.; Jeziorski, B. *Mol. Phys.* **1979**, *38*, 191.
(16) Jeziorska, M.; Jeziorski, B.; Cizek, J. *Int. J. Quantum Chem.* **1987**, *32*, 149.
(17) Moszynski, R.; Heijmen, T. G. A.; Jeziorski, B. *Mol. Phys.* **1996**, *88*, 741.
(18) Sadlej, A. J. *Mol. Phys.* **1980**, *39*, 1249.
(19) Jaszunski, M. *Mol. Phys.* **1980**, *39*, 777.
(20) Jeziorski, B.; Bulski, M.; Piela, L. *Int. J. Quantum Chem.* **1976**, *10*, 281.
(21) Moszynski, R.; Jeziorski, B.; Ratkiewicz, A.; Rybak, S. *J. Chem. Phys.* **1993**, *99*, 8856.
(22) Moszynski, R.; Jeziorski, B.; Szalewicz, K. *J. Chem. Phys.* **1994**, *100*, 1312.
(23) Moszynski, R.; Jeziorski, B.; Rybak, S.; Szalewicz, K.; Williams, H. L. *J. Chem. Phys.* **1994**, *100*, 5080.
(24) Rybak, S.; Jeziorski, B.; Szalewicz, K. *J. Chem. Phys.* **1991**, *95*, 6576.
(25) Moszynski, R.; Cybulski, S. M.; Chalasinski, G. *J. Chem. Phys.* **1994**, *100*, 4998.
(26) Chalasinski, G.; Jeziorski, B. *Theor. Chim. Acta* **1977**, *46*, 277.
(27) Moszynski, R.; Jeziorski, B.; Diercksen, G. H. F.; Viehland, L. A. *J. Chem. Phys.* **1994**, *101*, 4697.
(28) Moszynski, R.; Jeziorski, B.; Szalewicz, K. *Int. J. Quantum Chem.* **1993**, *45*, 409.
(29) Williams, H. L.; Szalewicz, K.; Moszynski, R.; Jeziorski, B. *J. Chem. Phys.* **1995**, *103*, 4586.
(30) Woon, D. E.; Dunning, T. H. *J. Chem. Phys.* **1995**, *103*, 4572.
(31) Basis sets were obtained from the Extensible Computational Chemistry Environment Basis Set Database, Version 1.0, as developed and distributed by the Molecular Science Computing Facility, Environmental and Molecular Sciences Laboratory which is part of the Pacific Northwest Laboratory, P.O. Box 999, Richland, WA 99352, and funded by the U.S. Department of Energy. The Pacific Northwest Laboratory is a multiprogram laboratory operated by Battelle Memorial Institute for the U.S. Department of Energy under Contract DE-AC06-76RLO 1830.
(32) Woon, D. E.; Dunning, T. H. *J. Chem. Phys.* **1994**, *100*, 2974.
(33) Diercksen, G. H. F.; Sadlej, A. J. *Chem. Phys.* **1985**, *96*, 17, 43.
(34) Jeziorski, B.; Moszynski, R.; Ratkiewicz, A.; Rybak, S.; Szalewicz, K.; Williams, H. L. SAPT: A Program for Many-Body Symmetry-Adapted Perturbation Theory Calculations of Intermolecular Interactions. In *Methods and Techniques in Computational Chemistry: METECC-94, vol. B Medium Size Systems*; Clementi, E., Ed.; STEF: Cagliari, 1993; p 79.
(35) Hettema, H.; Wormer, P. E. S.; Thakkar, A. J. *Mol. Phys.* **1993**, *80*, 533.
(36) Wormer, P. E. S.; Hettema, H. *J. Chem. Phys.* **1992**, *97*, 5592.
(37) Wormer, P. E. S.; Hettema, H. POLCOR package, Nijmegen, 1992.
(38) Boys, S. F.; Bernardi, F. *Mol. Phys.* **1970**, *19*, 553.
(39) Chalasinski, G.; Jeziorski, B. *Mol. Phys.* **1974**, *27*, 649.
(40) Knowles, P. J.; Meath, W. J. *Mol. Phys.* **1986**, *59*, 965.
(41) Knowles, P. J.; Meath, W. J. *Mol. Phys.* **1987**, *60*, 1143.
(42) Tang, K. T.; Toennies, J. P. *J. Chem. Phys.* **1984**, *80*, 3726.
(43) Moszynski, R.; Korona, T.; Heijmen, T. G. A.; Wormer, P. E. S.; van der Avoird, A.; Schramm, B. *Pol. J. Chem.*, submitted for publication.
(44) van der Avoird, A.; Wormer, P. E. S.; Moszynski, R. *Chem. Rev.* **1994**, *94*, 1931.
(45) Bratoz, S.; Martin, M. L. *J. Chem. Phys.* **1965**, *42*, 1051.
(46) Tennyson, J.; Sutcliffe, B. T. *J. Chem. Phys.* **1982**, *77*, 4061.
(47) Brocks, G.; van der Avoird, A.; Sutcliffe, B. T.; Tennyson, J. *Mol. Phys.* **1983**, *50*, 1025.
(48) Brink, D. M.; Satchler, G. R. *Angular Momentum*; Clarendon: Oxford, 1975.
(49) *Handbook of Chemistry and Physics*; Weast, R. C., Asth, M. J., Eds.; CRC Press: Boca Raton, FL, 1981.
(50) Varberg, T. D.; Evenson, K. M. *Ap. J.* **1992**, *385*, 763.